

Original Article

Design of a Mobile Manipulator Robot Prototype for Drilling in Underground Mining

Franco Iriarte-Zambrano¹, Alicia Rojas-Davila², Carlos Sotomayor-Beltran³, Jose Briones-Zuñiga⁴

^{1,2,3,4}Universidad Tecnológica del Perú, Lima, Perú.

⁴Corresponding Author : c19980@utp.edu.pe

Received: 23 July 2024

Revised: 21 March 2025

Accepted: 28 March 2025

Published: 26 April 2025

Abstract - This study presents the design and development of a mobile manipulator robot prototype intended for drilling in underground mining. The robot integrates a track-based traction system and a drilling arm, both controlled by a Raspberry Pi-based control unit. Equipped with LIDAR and proximity sensors, the robot can map and analyze its environment in real time, enhancing safety and efficiency in mining operations. The methodology includes kinematic and dynamic modeling of the system, using Denavit-Hartenberg and Euler-Lagrange equations and the simulation of movements and trajectories in MATLAB and RoboDK. This approach optimizes the robot's performance in hostile environments, reducing risks for workers and increasing productivity. The results indicate improved capacity to operate in extreme conditions, highlighting the feasibility of the robot for implementation in underground mining. This advancement promises a significant reduction in costs and improvement in safety, marking an important step towards automation in the mining industry.

Keywords - Robotic arm, Mining industry automation, Dynamic modeling, Underground mining, Safety enhancement.

1. Introduction

Currently, mining in Peru makes up 16% of the GDP [1]. Despite being a country with large mining deposits, mining minerals is still carried out manually. With the rise of technology, it is necessary to delve deeper to meet the demand, increasing human risk and the monetary and personal cost. According to the Ministry of Energy and Mines of Peru, from 2021 to 2023, a total of 145 victims of mining accidents were registered, of which 72 were fatal. A substantial increase in collapse accidents was also observed over the years, indicating that mineral extraction is increasingly dangerous [2].

The implementation of robots in mining not only benefits safety but also efficiency. These autonomous robots can work continuously and without fatigue [6], increasing efficiency in extraction and transportation and significantly reducing costs. This results in consistent production and less waste [3]. As postulated in [4], robots not only increase production and reduce risk but also minimize environmental impact. According to their designs, they can operate cleaner and more remotely, reducing the environmental impact linked to traditional mining. The use of robots in mining not only has the potential to improve safety and efficiency but also helps open opportunities for the exploration and extraction of minerals that are difficult to obtain in traditional ways [2, 4]. To achieve this, it is important to consider the technological and logistical challenges linked to these advancements to make the most of these resources.

Mining in Peru is one of the territory's main sources of income; however, unlike other mining countries, Peru still uses manual methods for extracting and handling minerals. In [4, 5], it is indicated that the main reasons for adopting these new technologies are work efficiency and personnel safety. Under this premise, it is expected that mining companies will opt for robotic automated systems to perform these tasks in the future. To begin, [7] explains that using robots in the mining field is relatively new but not unusual. The demand for rare minerals, accuracy, and precision are highly required by current standards. Additionally, using robots reduces human error and the health risks associated with working in these environments. In general, the prototype is based on three systems: the mobile system, the arm system, and the control system for the mobile system. A study [8] indicates that for the robot to be successful in confined or reduced spaces, it is necessary to apply a trajectory planning algorithm. Obstacle avoidance and precision are of vital importance if the robot is to be used for mining. [9] points out that trajectory planning alone is not enough; it must be supported by sensors and complemented by the operator's field training to achieve a symbiosis between the mechanical-autonomous part and the human part. For this study, the use of a robotic manipulator arm was chosen. Robotic manipulator arms were created to meet the need to automate jobs [10]. They earned their place in the industry by being programmable, able to work continuously, and having great loading capacity. According to [11], their main attraction is their capacity for modulation and



adaptability to the established industry. Depending on the control, they can be applied in remote autonomous tasks, as in this prototype. For the correct functioning of the proposed arm in this work, it is necessary to apply different approaches, parameters, and modulation. Regarding the control system, [12] offers an alternative based on a gesture recognition system using a wristband composed of nano optical fibers.

This will allow us to move the arm freely by copying the movements of the operator's hand. On the other hand, [13] provides a trajectory planning method based on swarm intelligence to manage and solve problems, providing optimal and rapidly converging solutions. Continuing with the control section, a research study [14] developed an improvement for the optimization of the thermal parameters in the joints of the manipulator, specifically in the rotors. This model allows for reducing the energy cost of cooling the joints. For [15], positioning error is vital, so they developed a self-compensation method to reduce this error using a dynamic fuzzy neural network. In both cases, the authors present a tentative parameter improvement to apply in underground environments, where optimizing features is of utmost importance.

Finally, there is a consensus on the importance of applying robots to support and improve human work efficiency. In this case, mining robots can work for longer periods compared to a human who requires oxygen and is exposed to the danger of collapse and the fatigue of heavy work. The present work seeks to reduce the risk associated with underground mining, increase extraction efficiency, reduce costs, and increase production. The proposed design aims to meet these needs by combining the mechanical-automatic and manual control parts to achieve an optimal result.

2. Methodology

2.1. Mathematical Modeling

As a first step, the kinematic and dynamic models of both the caterpillar and the arm were obtained by applying the Denavit-Hartenberg methods, the Euler-Lagrange dynamic analysis, and the torque equations required for the prototype.

2.1.1. Kinematic Analysis of the Manipulator Arm

As explained in [16], the kinematic model of a Cartesian manipulator robot is described as the positions of the coordinates in a three-dimensional space applied to the ends of the arm to relate the positions of its joints.

Based on this, we first adapt our model to a kinematic diagram observable in Figure 1 to apply the Denavit-Hartenberg convention. In Figure 1, 4 revolute joints are represented, Z0 is a vertical revolute type, and the axes Z1, Z2, and Z3 are horizontal revolutes; the length of the links between Z axes is represented by L1, L2, L3, L4 and the angles q1, q2, q3, q4 represent the θ variables.

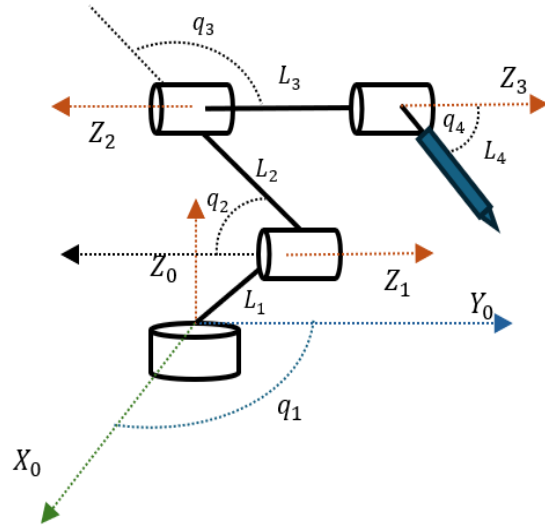


Fig. 1 Kinematic sketch of the arm

Table 1. Denavit Hartenberg table of 4 DOF

j	α_i	α_j	d_j	θ_i
J1	0	$\pi/2$	L1	θ_1
J2	L2	0	0	θ_2
J3	L3	0	0	θ_3
J4	L4	0	0	θ_4

Table 1 shows the data collected from Figure 1. J1, J2, J3, and J4 are the sections where the Cartesian coordinates are evaluated, α_i represents the distance between the Z axes, α_j represents the angle that needs to be rotated to align the Z axes, d_j represents the displacement on the x-axis for these to coincide, and finally, θ_i represents the variable angles of the entire system.

$$A_j = \begin{bmatrix} C\theta_i & -S\theta_i C\alpha_i & S\theta_i S\alpha_i & \alpha_i C\theta_i \\ S\theta_i & C\theta_i C\alpha_i & -C\theta_i S\alpha_i & \alpha_i S\theta_i \\ 0 & S\alpha_i & C\alpha_i & d_j \\ 0 & 0 & 0 & 1 \end{bmatrix} \quad (1)$$

By replacing the values from the table in Equation 1, four homogeneous transformation matrices are obtained that help us find the position of the manipulator with respect to the end effector, represented below as Equations 2, 3, 4 and 5.

$$T_1^0 = \begin{bmatrix} C1 & -S1 & 0 & 0 \\ S1 & C1 & 0 & 0 \\ 0 & 0 & 1 & L1 \\ 0 & 0 & 0 & 1 \end{bmatrix} \quad (2)$$

$$T_2^1 = \begin{bmatrix} C2 & -S2 & 0 & L2C2 \\ S2 & C2 & 0 & L2S2 \\ 0 & 0 & 1 & 0 \\ 0 & 0 & 0 & 1 \end{bmatrix} \quad (3)$$

$$T_3^2 = \begin{bmatrix} C3 & -S3 & 0 & L3C3 \\ S3 & C3 & 0 & L3C3 \\ 0 & 0 & 1 & 0 \\ 0 & 0 & 0 & 1 \end{bmatrix} \quad (4)$$

$$T_4^3 = \begin{bmatrix} C4 & -S4 & 0 & L4S4 \\ S4 & C4 & 0 & L4S4 \\ 0 & 0 & 1 & 0 \\ 0 & 0 & 0 & 1 \end{bmatrix} \quad (5)$$

$$T = T_1^0 * T_2^1 * T_3^2 * T_4^3 \quad (6)$$

Once the four homogeneous transformation matrices are obtained, we proceed to multiply them using equation 6 to find the relationship of the links with the base.

This is of utmost importance for the simulations, the control of the arm and the following dynamic mathematical calculations of the robot manipulator.

2.1.2. Dynamic Analysis of the Manipulator Arm

Once equation 1 is obtained, calculations of the tensor matrix known as the Euler-Lagrange method [16] were carried out. To begin, we must calculate the kinetic energies and the partial derivatives they exert on the model based on Equation 1. Once these were obtained, potential energies were calculated, always based on the previous systems of equations.

Once these unknowns are resolved, we proceed to formulate the Lagrange equation ($L = T - V$), which is represented as the difference between the kinetic energy and the potential energy. Once this new system is obtained, equation 3 is applied to each generalized coordinate. With this, a system of second-order equations was obtained, and to finish, we solved the equations obtained to find the functions $\tau(i)$, which represent the temporal dynamics of the robot.

$$\tau_1 = -d\theta_2 * (L2 * L4 * d\theta_1 * m4 * \sin(\theta_2 + \theta_3) + (L2 * L4 * d\theta_2 * m4 * \sin(\theta_2 + \theta_3))/2 + (L2 * L4 * d\theta_3 * m4 * \sin(\theta_2 + \theta_3))/2 + L2 * L3 * d\theta_1 * m3 * \sin(\theta_2) + 2L2 * L3 * \theta_1 * m4 * \sin(\theta_2) + L2 * L3 * d\theta_2 * m3 * \sin(\theta_2))/2 + L2 * L3 * d\theta_2 * m4 * \sin(\theta_2)) - d\theta_3 * (L2 * L4 * d\theta_1 * m4 * \sin(\theta_2 + \theta_3) + (L2 * L4 * d\theta_3 * m4 * \sin(\theta_2 + \theta_3))/2 + (L2 * L4 * d\theta_3 * m4 * \sin(\theta_2 + \theta_3))/2 + L3 * L4 * d\theta_1 * m4 * \sin(\theta_3) + L3 * L4 * d\theta_2 * m4 * \sin(\theta_3) + (L3 * L4 * d\theta_3 * m4 * \sin(\theta_3))/2) \quad (7)$$

$$\tau_2 = (L2 * L3 * d\theta_1^2 * m3 * \sin(\theta_2))/2 + L2 * L3 * d\theta_1^2 * m4 * \sin(\theta_2) - (L3 * L4 * d\theta_3^2 * m4 * \sin(\theta_3))/2 + (L2 * L4 * d\theta_1^2 * m4 * \sin(\theta_2 + \theta_3))/2 - L3 * L4 * d\theta_1 * d\theta_3 * m4 * \sin(\theta_3) - L3 * L4 * d\theta_2 * d\theta_3 * m4 * \sin(\theta_3) \quad (8)$$

$$\tau_3 = (L4 * m4 * (L2 * d\theta_1^2 * \sin(\theta_2 + \theta_3) + L3 * d\theta_1^2 * \sin(\theta_3) + L3 * d\theta_2^2 * \sin(\theta_3) + 2 * L3 * d\theta_1 * d\theta_2 * \sin(\theta_3)))/2 \quad (9)$$

$$\tau_4 = 0 \quad (10)$$

The taus, denoted as $\tau(i)$, shown in Equations 7, 8, 9 and 10, represent the forces that must be applied to each of the robot's joints to achieve the desired movement [16]. Specifically, $\tau(1)$ represents the torque necessary in the first joint to generate the movement corresponding to $\theta(1)$.

Similarly, $\tau(2)$ represents the torque necessary in the second joint to generate the movement corresponding to $\theta(2)$; $\tau(3)$ represents the torque necessary in the third joint to generate the movement corresponding to $\theta(3)$, and $\tau(4)$ represents the torque necessary in the fourth joint to generate the movement corresponding to $\theta(4)$. In summary, $\tau(i)$ are the forces required by each robot joint to produce movement, compensating for gravitational, inertial, and any external forces exerted on the robot.

2.1.3. Dynamic Analysis of the Track System

As indicated in 2 studies [17] [18], the incorporation of a suspension system in a caterpillar-type traction robot is of utmost importance since the robot's trajectory includes obstacles that could affect the proper contact between the caterpillars and the ground, resulting in instability of the robot. Therefore, the formulation of a mathematical model that has the ability to represent the suspension system was carried out. To create this model, two points located at the centers of the radius of curvature of each caterpillar are strategically chosen.

This is done to analyze the dynamic behavior of the robot in relation to its trajectory. The selected points are chosen based on their location, where greater displacement is experienced when overcoming obstacles. The main objective of this choice is to obtain the necessary stiffness and viscosity coefficients for the efficient design of the track system. To analyze the dynamic behavior, a reference system is used where its center of gravity is located, and this system is used to determine the relative positions of the points of interest.

Subsequently, the lateral (Y) and vertical (Z) displacements are examined, and the angular displacement related to the X and Y axes is also represented, giving rise to the roll and pitch angles, respectively. In this way, the movement of both the suspended mass and the unsuspended masses associated with each analysis point is investigated [17, 18]. The diagram shown in Figure 2 presents a 12 DOF model considering the displacements in Z and Y of each of the reference points and the rigid body (ms), as well as the consideration of the pitch (θ) and roll angles (ϕ).

The presence of the weight of both the mass and the suspended system causes a downward movement in the vertical Z axis. Next, it is necessary to examine the forces affecting the system. Furthermore, when there is an angle of inclination, a lateral displacement with respect to the Y axis is generated, which also requires detailed analysis [17].

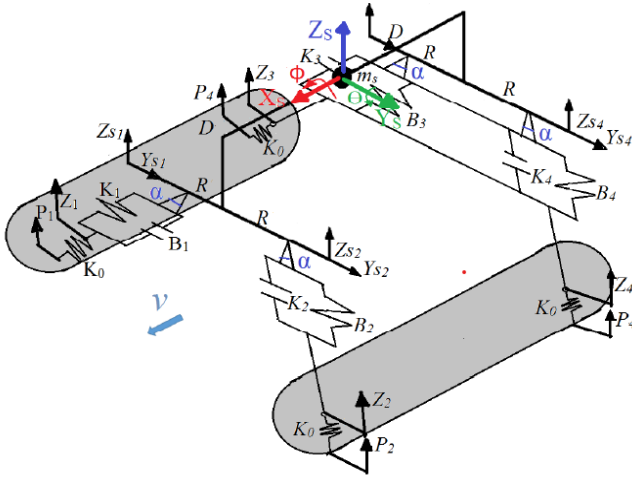


Fig. 2 Parametric scheme of the track system

Following the methodology of [17], the unsuspended mass with respect to the vertical Z axis was analyzed. To carry out this analysis, each reference point (1, 2, 3, 4) is considered, as shown in Figure 2, always considering the angle of inclination generated by the opening of the tracks. After completing the scheme, the equations of the forces associated with the system are derived. Then, the vertical Z axis is analyzed for a suspended mass. To do this, the forces that directly affect the mass are considered, obtaining equations that relate the forces that operate with the four reference points. Once these calculations have been made, the lateral Y axis for a mass was analyzed. To achieve this, the variation in the direction of the operating forces between the odd and even points was considered. To finish, we analyze the lateral Y axis for a suspended mass. This is obtained by evaluating the forces that affect the suspended mass. After carrying out all these analyses, the systems of equations are solved, obtaining Equation 11.

$$I_{\phi} \ddot{\phi} = -4BR^2(\cos\alpha)\dot{\phi} - 4KR^2(\cos\alpha)\phi - BR(\cos\alpha)\dot{Z}_1 - KR(\cos\alpha)Z_1 + BR(\cos\alpha)\dot{Z}_2 + KR(\cos\alpha)Z_2 - BR(\cos\alpha)\dot{Z}_3 + KR(\cos\alpha)Z_3 + BR(\cos\alpha)\dot{Z}_4 + KR(\cos\alpha)Z_4 \quad (11)$$

2.1.4. Torque Calculation

As observed in equation 12, in our case, the torque refers to the rotational force necessary to overcome the resistance of the load, and the angular velocity is the rotation speed required to do the work. For specific applications, it is essential to know the load speed requirements to determine the required motor power. Furthermore, the motor efficiency must be considered to calculate the actual power required at the motor input [17].

$$T = \frac{1}{2} m(\text{radius})^2 * \text{RPM} * \frac{2\pi \text{rad}}{\text{REV}} * \frac{1 \text{min}}{60 \text{s}} \quad (12)$$

In this work case, to obtain the variables, we will use the prototype by applying CAD design software, such as

Autodesk Inventor and Solidworks, to accurately calculate the torque required by the system. The data recovered from the CAD software was applied, as well as the RPM for the prototype, which will be low since more load capacity is needed than speed.

2.1.5. Required Engine Power

The calculation of the required power of a motor depends on several factors, such as the load that must be moved, the desired speed, the efficiency of the motor and other specific parameters of the application, [19] provides us with Equation 13, which relates the torque obtained in Equation 8 with angular velocity.

$$P_{req} = T * \omega \quad (13)$$

2.1.6. System Efficiency

To calculate the efficiency, our calculations were based on [19], which states that calculating the efficiency required by the motor involves determining how efficient the motor must be in a specific application to meet the performance and energy consumption requirements. The efficiency of a motor is calculated as the ratio between the useful output power and the input power. Equation 14 shows the general formula applied.

$$\eta = P_M / P_E \quad (14)$$

Breaking down Equation 11, η becomes the required efficiency. The useful output power is the power the motor must provide to do the required work, while the input power is the electrical energy the motor consumes. The efficiency value is usually expressed as a percentage (%). To calculate the required efficiency, the desired useful output power and the estimated or available input power must be known.

2.1.7. Calculation of Load Capacity

From [20], Equation 15 is obtained to calculate the load capacity; in general terms, load capacity depends on application and can vary widely.

$$CC_p = F_p * F_s \quad (15)$$

Where CC_p is the maximum load capacity, F_p is the maximum allowable force that the system can withstand without being damaged, and F_s is the safety factor value that guarantees safety. This value depends on the utility given to the robot as it is around.

2.2. Trajectory Planning

Trajectory planning is of utmost importance for an autonomous robot intended for mining; this is a crucial process since it allows the robot to go from point A to B without human control, avoiding obstacles and collisions [8]. This process is carried out by representing the environment in a 2D or 3D manner, depending on the

algorithm or sampling method and/or sensors used; in this case, a LIDAR sensor and an ultrasonic sensor will be applied to detect the environment once the environment is obtained, we proceed to use the algorithm that best suits the problem, such as Probabilistic Road Maps (PRM) (Figure 4) or Rapidly-exploring Random Trees (RRT), once the algorithm to be used has been chosen, the route is optimized taking into account the limitations of the robot, this is done to reduce the energy cost and the time it takes to reach its destination. If it has a changing environment, collision avoidance algorithms such as Vector Field Histogram (Figure 3) or Dynamic can also be used. Window Approach (DWA) provides us with the security that the robot reaches its destination safely and quickly [21].

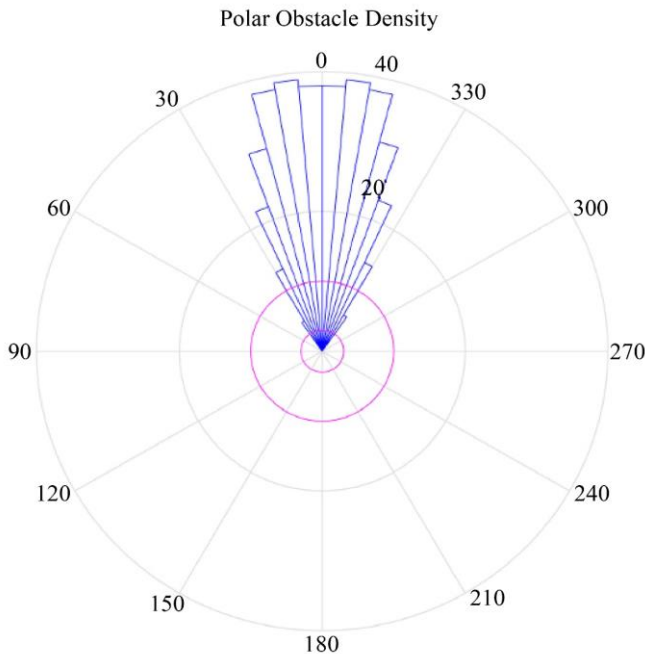


Fig. 3 Vector field histogram (VFH)

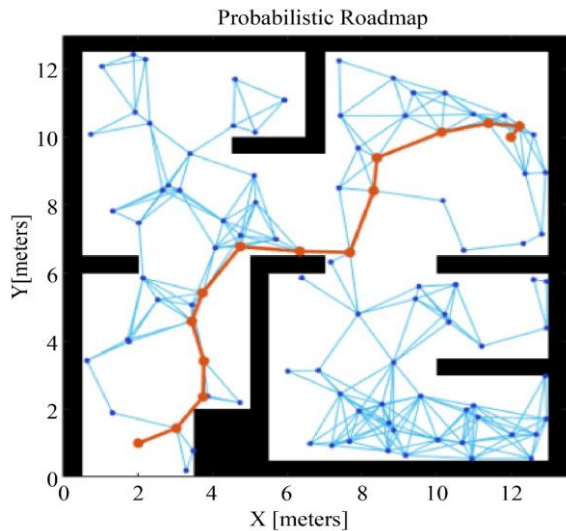


Fig. 4 Probabilistic roadmaps (PRM)

2.3. Robot Operating Diagrams

2.3.1. Track System Operation Diagram

Figure 5 shows the general operating diagram of the tracked movement system (moving part of the robot). This system is initialized before the arm system since it is essential for the correct functioning and movement of the entire robot.

Overall, the system begins by receiving a control signal from the control room, then turns on the motors, and the process of reviewing the location system begins to evaluate where the robot is, followed by sensor calibration of the proximity sensors to detect that the robot has a free path and does not collide with anything.

Once this has been verified, the temperature sensors begin their verification, after which all the data obtained returns to the control room in the form of feedback.

2.3.2. Drilling Arm Operating Diagram

In Figure 6, the operation of the drilling manipulator arm is generally presented. It begins with a control signal, which turns on the arm and sends it to the configured initial position.

Afterwards, the system runs a sensor positioning check to ensure it is effectively in the initial position; after this, the temperature sensors are run to ensure no anomaly; subsequently, all this data is entered in the form of feedback back to the control room.

2.3.3 Prototype Block Diagram

Once the torque in Equation 12, the required power in Equation 13, the system efficiency in Equation 14 and the load capacity in Equation 15 have been calculated, and these components were interconnected, as well as the sensors that will accompany them and, are observed in Figure 7.

Firstly, a power source is needed; the prototype will have a battery with sufficient voltage and amperage to supply both the tracked mobile system and the manipulator arm system.

Secondly, it can be seen in Figure 7 that a microcontroller will oversee the complete control of both systems; this will be supported by proximity, temperature, location and LIDAR sensors to be able to work correctly.

These sensors will provide the microcontroller with the necessary data to locate obstacles, the exact positioning of where they are in the mine, and the temperature of the joints of the manipulator's arm to avoid energy waste.

Additionally, a remote control system will be implemented to control the arm in a more precise way through remote control with gesture recognition. This will be helped by cameras installed in the robot, and finally, all this sensor data can be seen on the LCD screen so that the operator can monitor the robot's operation.

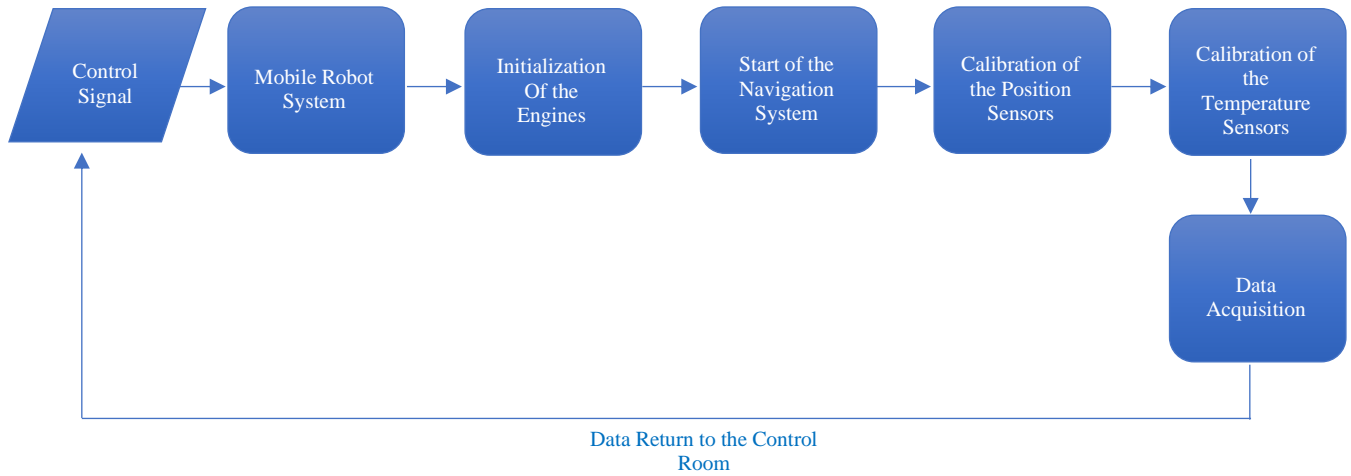


Fig. 5 Track system operation diagram

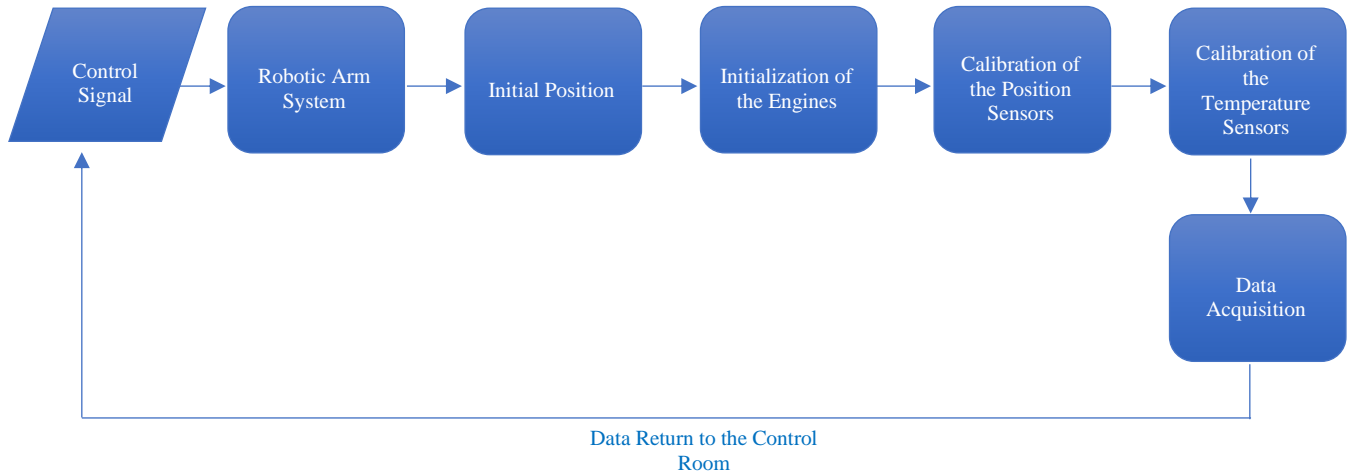


Fig. 6 Drilling arm operating diagram

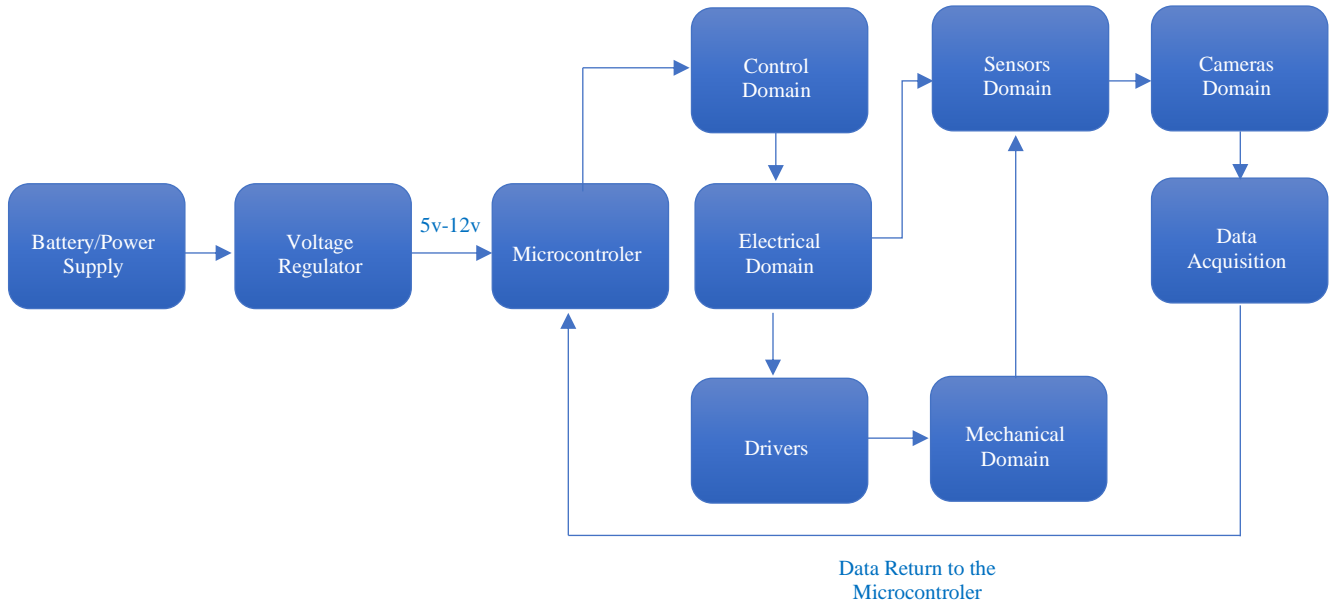


Fig. 7 System operation diagram

2.4. Component Selection

2.4.1. Engine Selection

For the selection of the engine, the CAD designs of the prototype were considered, the results of Equations 9, 10, 11, 12 and the parameters observable in [3, 7, 17], taking into consideration the above for the entire system. Two types of motors will be used: electric motors, Servomotors (Figure 8) and Stepper Motors (Figure 9); these will allow us better control and, in turn, reduce the environmental impact compared to combustion engines.



Fig. 8 Servomotor



Fig. 9 Stepper motor



Fig. 10 Driver L293D

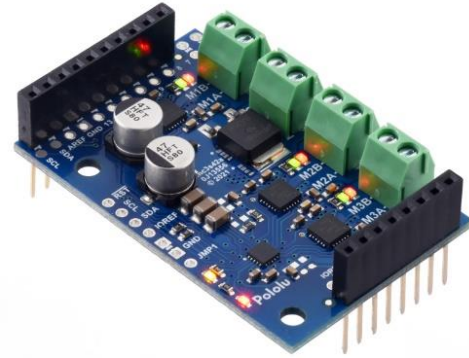


Fig. 11 Driver motor M3S256

2.4.2. Driver Selection

Regarding the selection of drivers, since two systems are present, the mobile system and the arm system, for the mobile system, the L293D driver will be used (Figure 10), which controls two motors, and two Motor drivers M3S256 (Figure 11), which can control 3 motors for the arm system.

2.4.3. Power Source Selection

Once we select the number of motors required, the drivers and the control system, the total energy the prototype will consume can be calculated. In addition, for safety and reserve reasons, the battery capacity will be oversized. A battery capacity of 40AH is estimated.

2.4.4. Microcontroller Selection

For the selection of the microcontroller, the system requirements were considered; in our case, the prototype has 8 motors, 4 cameras, and several sensors, including the LYDAR; therefore, the selected microcontroller requires having multiple inputs, including inputs dedicated to cameras and a medium degree of computing capacity. The selected microcontroller is a Broadcom BCM2712, which is the CPU of the Raspberry Pi 4 (Figure 12). It will provide all the mentioned features and some extra ones for future improvements.



Fig. 12 Raspberry Pi 4

2.4.5. Voltage Regulator Selection

By having several voltage inputs for each device, it is of utmost importance to obtain a voltage regulator to provide the correct voltage to the components. In our case, the use of the LM2596 was opted for, which can be seen in Figure 13, which supports from 5V to 24V input and supplies 12V to 32V output, with an efficiency of 94.1% to 96.4%.



Fig. 13 LM2596 voltage regulator

2.4.6. Sensors Selection

For the temperature sensors, 3P12 mineral insulation thermocouples will be used. These sensors have IP67 protection, which makes them ideal for work where the environment is humid and/or with liquid splashes. These will help control the temperature at the joints. To reduce energy expenditure on cooling. For the lateral proximity sensors, the MB7360 HRXL-MaxSonar-WR will be used, and these infrared sensors have a vision range of 30cm to 5m at 7.5hz; they are analog and have IP67 protection; these will be used to avoid lateral collisions with rocks or other objects. It is also of utmost importance to verify that the hydraulic systems have the proper pressure; due to this, the SCP01 pressure sensors will be used, which are compact, have high resistance, and have a long useful life. In addition to these sensors, the prototype will have a navigation and location system and a LIDAR sensor. For navigation, a VN-200, which is a compact and high-performance system based on GNSS-INS, will be used.



Fig. 14 SLAM method in underground mining

It combines a 3-inch gyroscope axis, accelerometers and magnetometers, along with high-sensitivity GNSS, all controlled by the advanced Kalman filtering algorithm to provide optimal position, speed and altitude values.

As for the LIDAR system, the OS1 will be used; this model is a medium-range type of compact size and can generate 5.2 million points per second; it uses the SLAM mapping method (Figure 14) to locate and create a map of the environment simultaneously.

2.5. Hardware Design

Once all the components are selected, they are digitally represented for implementation, and a new reference scheme is created where the different systems will intercommunicate. Figures 15, 16 and 17 present the main components selected for the prototype, relating to the electrical, control, mechanical and vision domains.

The electrical domain includes the power supply and energy distribution systems; in the mechanical domain, the motors that support the moving parts of the robot are observed; in the control domain, the main control unit, in our case, the Raspberry Pi, can be observed and in the vision domain the LIDAR is present, cameras and HMIs for diagnosis and sensor visualization.

Figure 15 shows the relationship between the arm's control domain, the mechanical domain, and the mobile track system. In the case of the track system, 2 DC motors were used and linked to the L293D driver, which can control 2 motors simultaneously.

These are connected to the respective pins of the Raspberry Pi. For the arm system, 3 servos and 1 stepper motor were required, represented in the lower part of the figure.

Figure 16 shows the operating diagram of integrating the control domain with the vision domain without considering the LIDAR sensor.

This section has a camera (in this case virtual), a button that starts the program and a Display where the data obtained from the camera will be reflected, in addition to the respective connections to the Raspberry Pi so that the operator can take control of the environment in real time.

Figure 17 shows the interaction of the control domain and the sensor domain. In this case, only the temperature sensors of the 4 joints of the arm are represented.

The MCP3208 module is responsible for transforming the data sent by the sensors into data acceptable by the Raspberry Pi, which will later be visible on the LCD2.

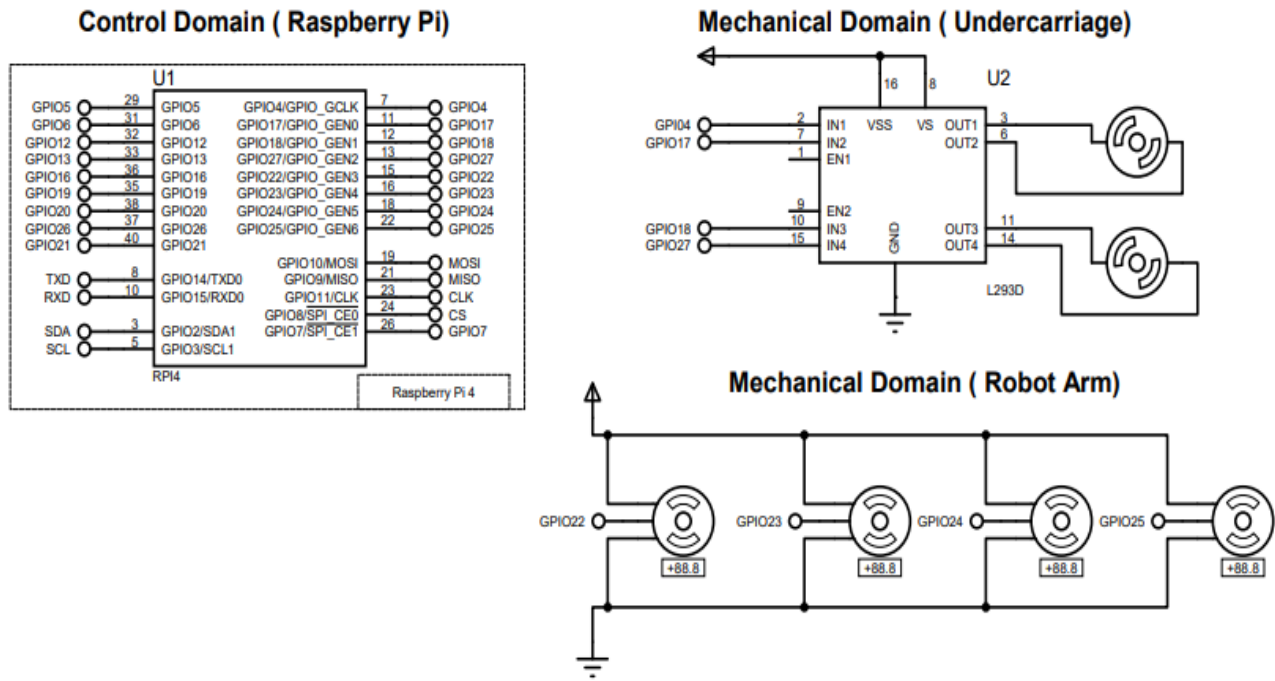


Fig. 15 Electromechanical operation and control diagram

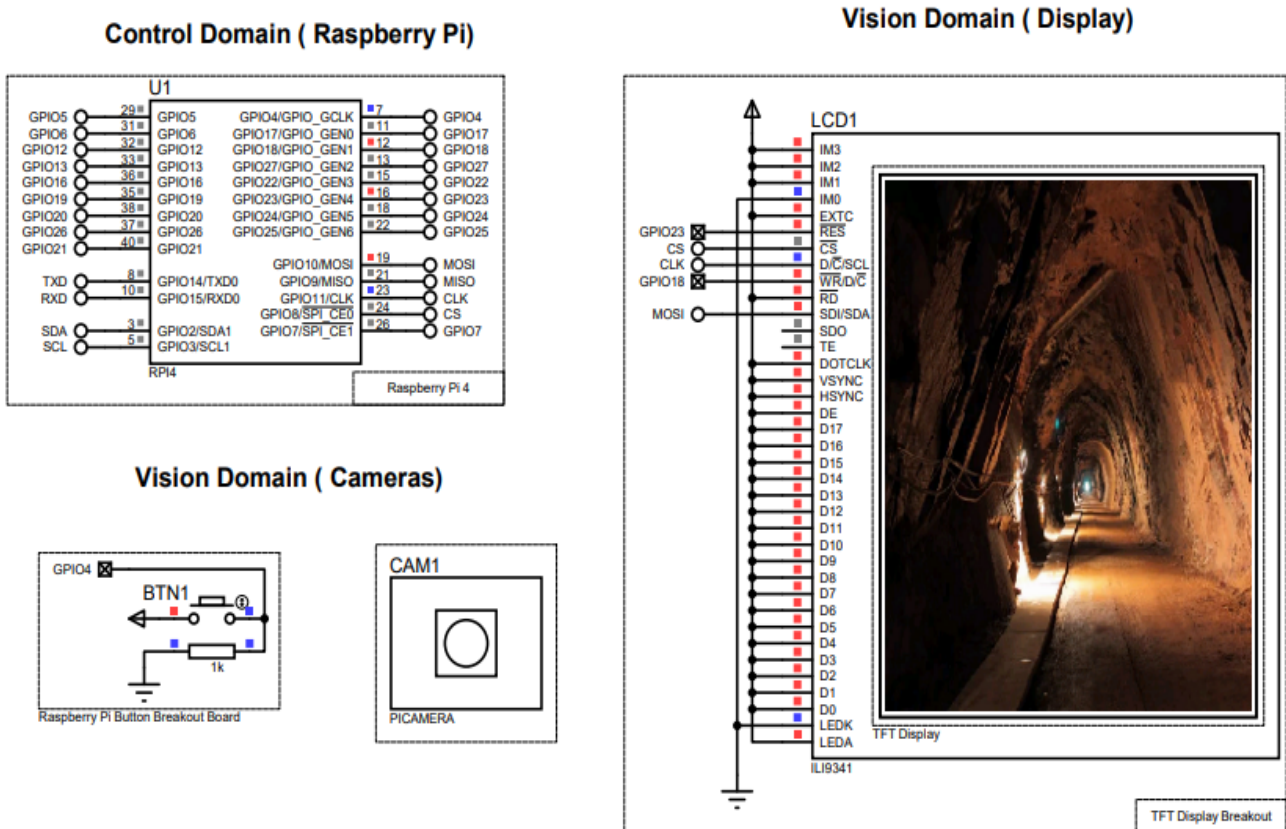


Fig. 16 Control and vision operation diagram

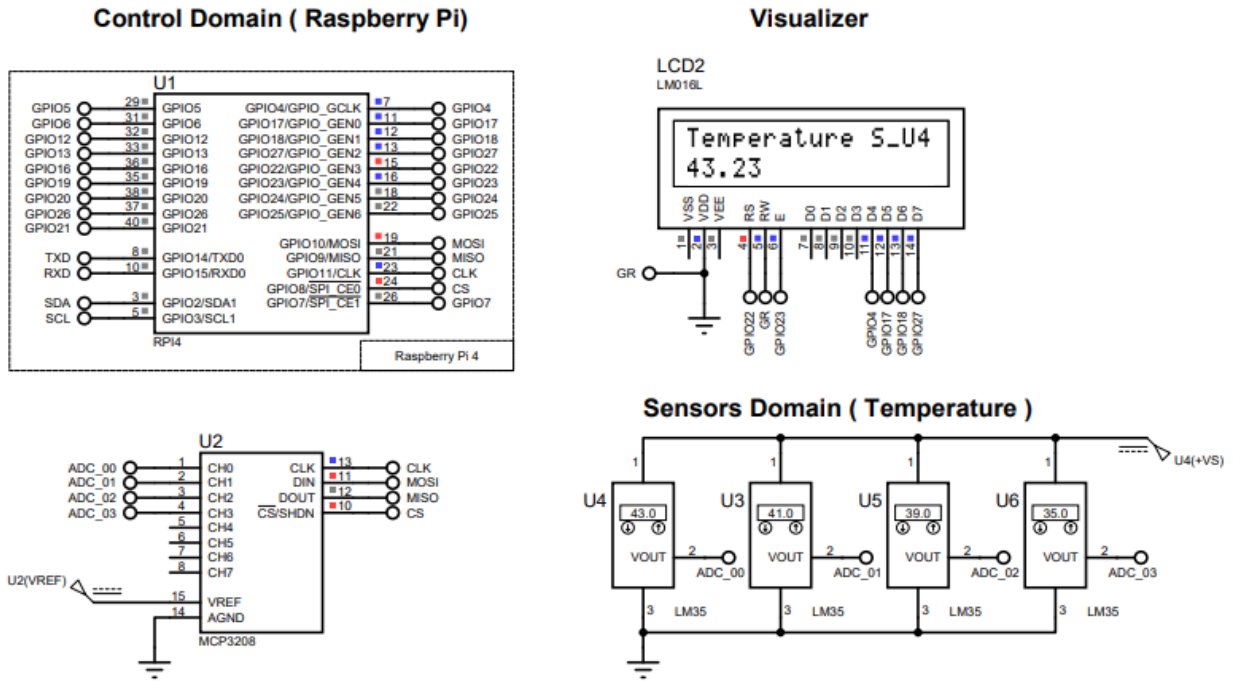


Fig. 17 Sensor domain operation diagram

2.6. Mechanical Design

The design proposed in Figure 18 focuses on integrating mobility, safety, and precision to perform drilling tasks in underground mining. The robot is equipped with a robust tracked locomotion system, capable of moving on different surfaces and overcoming obstacles. The 4 DOF articulated drilling arm allows precise drilling in specific locations, adjusting to different depths and angles according to the operator's requirements. Additionally, the design incorporates advanced sensors such as LIDAR for navigation and arm positioning, ensuring exact control and minimization of errors. Combining these features makes it a versatile and efficient tool for the previously mentioned applications.

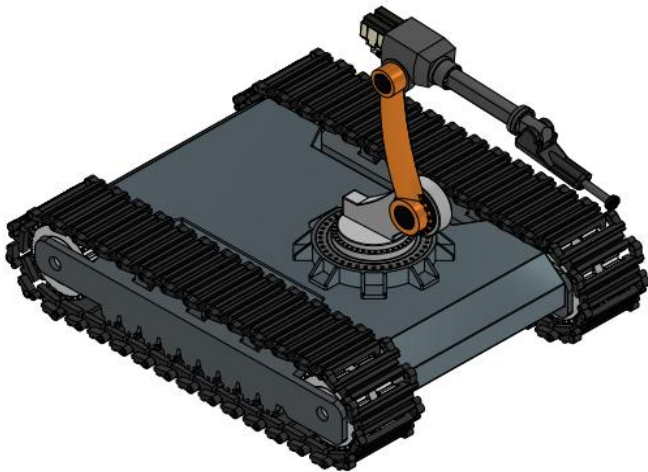


Fig. 18 Integrated design of the prototype

2.6.1. Mobile Unit Design

For the design of the moving part with tracks (Figure 19), we aimed to optimize efficiency and safety in difficult and hostile environments. The prototype features a tracked traction system that provides stability and power to navigate irregular, narrow terrain typical of underground mines. It is equipped with two rear-mounted AC motors, four proximity sensors (two on each side), a camera system, and a LIDAR sensor. This setup enables the robot to map and analyze its environment in real-time, avoiding obstacles and dangers. The robot's structure is robust and resilient, designed to withstand extreme conditions such as high humidity, variable temperatures, and dust.

It also possesses capabilities for loading and manipulating materials. Additionally, a remote monitoring system has been incorporated, allowing operators to control the robot from a safe location. The data collected by the LIDAR and cameras are processed by artificial intelligence algorithms, enhancing the efficiency of autonomous navigation. The incorporation of AI algorithms not only allows for real-time obstacle avoidance but also optimizes the robot's path planning, making it more efficient in task execution. The system can learn and adapt to different environmental conditions, improving its performance over time. Furthermore, the robot's design includes a modular component system, enabling easy maintenance and upgrades and ensuring the robot can adapt to future technological advancements. Safety features are paramount, with multiple fail-safes and redundant systems to ensure the robot operates reliably under all conditions.

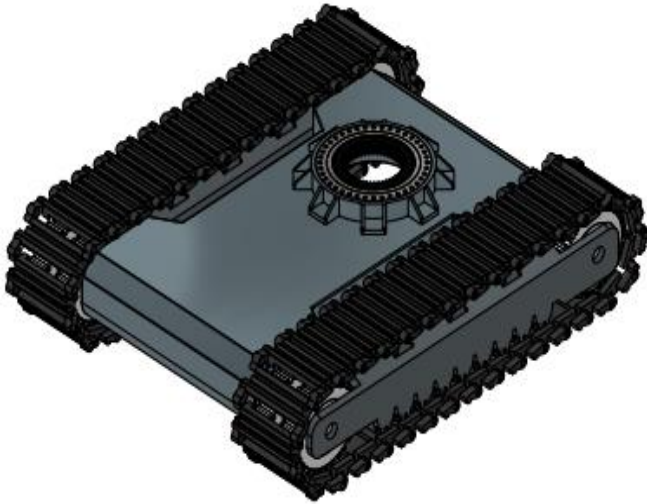


Fig. 19 Mobile unit design

Integrating advanced sensors and robust communication systems ensures continuous operation, even in areas with limited connectivity. This comprehensive approach to design and functionality makes this prototype a versatile and reliable tool for the demanding conditions of underground mining, significantly enhancing both safety and productivity.

2.6.2. Drilling Arm Design

The design presented in Figure 20 focuses on precision, adaptability and control in demanding environments; a robotic arm was proposed with four joints that allow a wide range of movements, ensuring the ability to drill at specific angles and depths according to the needs of the terrain, this is equipped with three servos, a stepper motor for angular control of the base, four temperature sensors at the joints and an auxiliary camera for precision movements. Its construction is robust and durable, and it is prepared to withstand dust and humidity.



Fig. 20 Drilling arm design

2.7. Software Development

Once the design and selection of components were completed, the programming of the microcontroller was developed; for this, all the previously explained domains and their integrations were considered. Each section has a different type of control. Using the Raspberry Pi control unit, the software initializes and configures the GPIO pins, sensors, and actuators. In a main loop, the program continuously reads data from sensors such as LIDAR, proximity, and temperature to process this information, map the environment and detect obstacles. Based on this data, decisions are made to control the DC motors responsible for the robot's mobility and the servos that operate the drilling arm.

Additionally, the system can adjust camera settings for manual driving and monitor battery status to ensure safe operation. The code can also include communication functionalities to transmit data to a remote control and receive manual commands, ensuring real-time monitoring and control. Figure 21 shows the main program of the microcontroller. It begins with the initialization of all the critical systems of the mobile robot, including the configuration of the GPIO pins on the Raspberry Pi and the detailed configuration of the sensors and actuators. Once established, the code enters a main loop that runs continuously, ensuring constant monitoring of the environment by reading data from LIDAR, proximity sensors and temperature sensors. Within the loop, the collected data is processed to perform critical tasks such as obstacle detection, environment mapping, and active component temperature monitoring.

Based on this processed information, the program makes automated decisions that include adjusting the movement path of the mobile base, controlling the drilling arm to execute specific tasks, and adjusting the camera system settings to optimize vision and manual operation. Additionally, battery health check routines are implemented to ensure efficient power management and, if necessary, data transmission to a remote control is enabled for additional monitoring and control operations.

2.8. Simulators

To carry out component testing, design and carry out the algorithms, different simulators were used. Matlab was used to begin with for complex calculations of kinematics and dynamics and later to simulate obstacle avoidance and trajectory planning algorithms. Python was also used in the Pycharm and Visual Studio Code environments to carry out the simulations of the arm, Obstacle avoidance and the LIDAR. Additionally, RoboDK robot simulation software was used to visualize how the arm behaves in a controlled environment and evaluate if it does not have collisions. These simulators allowed for iterative testing and refinement of the algorithms, ensuring the highest level of precision and reliability in the robot's performance under various conditions.

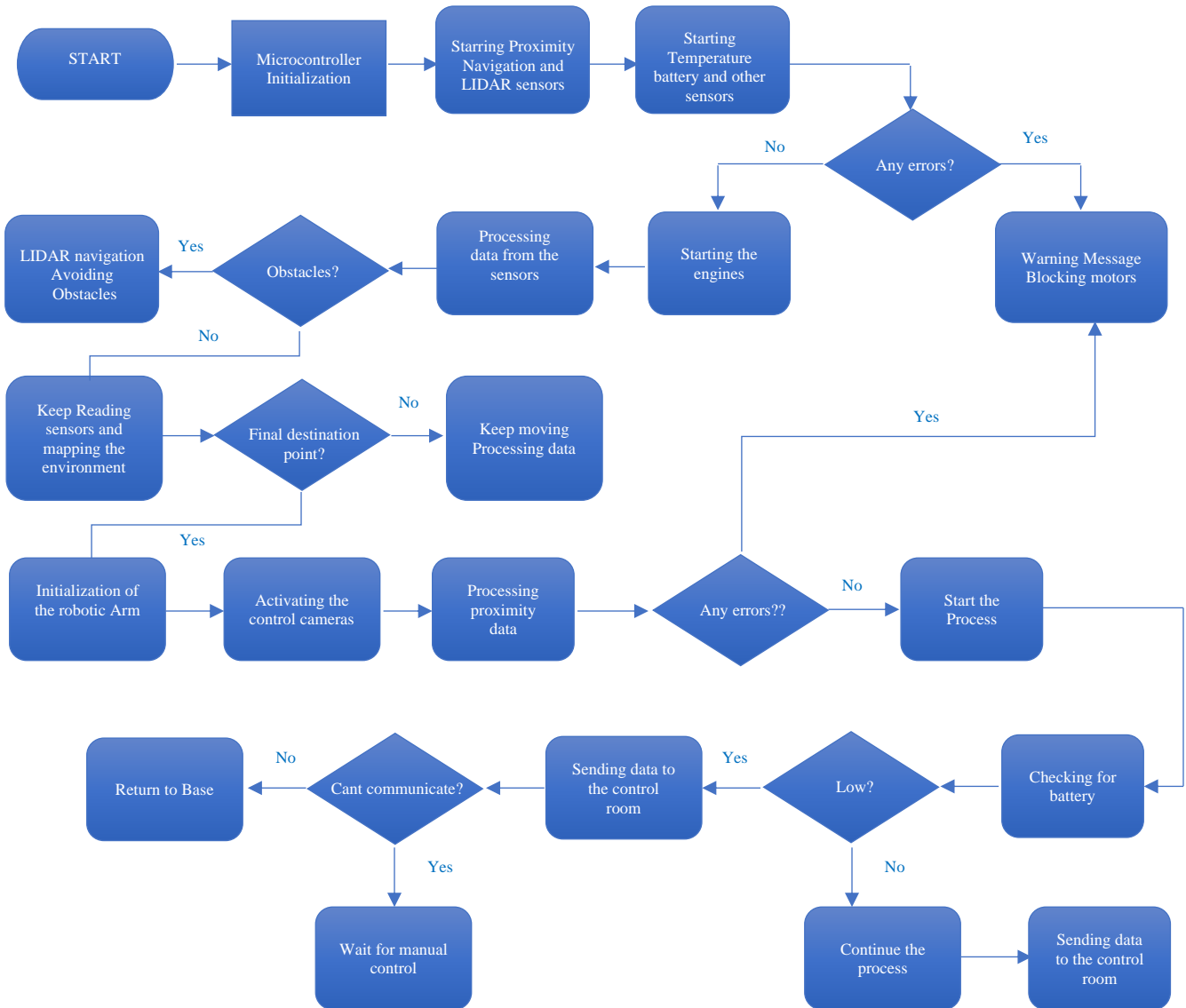


Fig. 21 Main flow chart of the microcontroller

3. Results and Discussion

3.1. Results

Once the CAD designs of the robot were obtained, the necessary torque was calculated using Equation 12, which gave an approximate value of 700 Nm. This calculation is crucial to properly size the actuators and ensure the robot can move and perform planned tasks effectively without overloading the motors. Furthermore, it was derived that, to support this torque, a power of 13.1 kW will be required, thus ensuring that the system can operate with the energy necessary for its functions. To guarantee the robustness and versatility of the robot, it was decided to oversize the maximum load capacity to 120 kg, which provides sufficient margin to handle unexpected conditions or additional loads during operation. This strategic approach will optimize the robot's performance and increase its operational capacity and reliability in various environments and applications.

For the trajectory planning section, it was found necessary to opt for LIDAR simulation since obtaining one is difficult and has a high cost. Using algorithms in Python, the LIDAR environment in 2D, as shown in Figure 22, could be recreated.

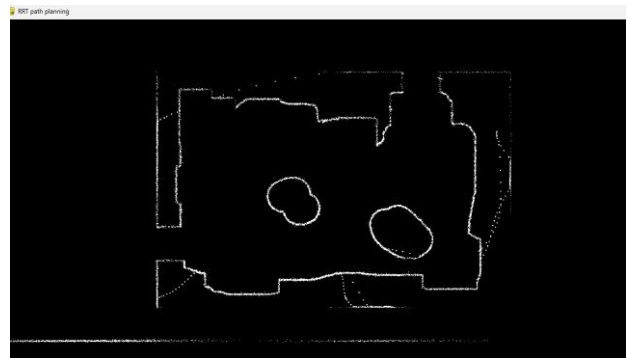


Fig. 22 2D environment simulation using LIDAR SLAM

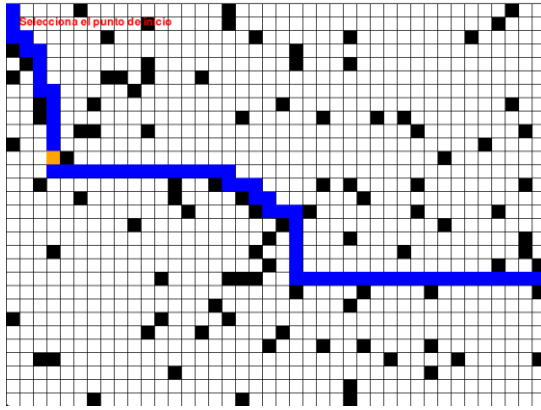


Fig. 23 Simulation of the RRT algorithm version 1

Figure 22 shows an environment simulating a cave with irregular walls and obstacles in the center. For areas of versatility in the simulation, the mouse cursor becomes the robot. As it moves through the environment, it maps its path with the laser, and this, when bouncing off the sensor, creates a point, and this is how it manages to navigate the environment; however, mapping is not enough for the robot to be autonomous, it needs an algorithm that translates this data and manages to evade obstacles, and that it allows you to get from point A to B autonomously, relying on LIDAR as your vision. The prototype also has an RRT obstacle avoidance algorithm to achieve this, as shown in Figure 23.

As seen in Figure 23, the obstacle avoidance algorithm is fundamental in the autonomous navigation of this type of robot; it guarantees safe and efficient movement in dynamic and unknown environments. In our case, the algorithm uses data from the LIDAR sensor and proximity sensors to detect nearby obstacles in the robot's environment. Once detected, it calculates alternative trajectories that allow the robot to avoid obstacles while staying en route to its destination. This means it dynamically generates routes based on criteria such as distance to the obstacle, speed, and the robot's maneuverability. In addition, the algorithm can also integrate other trajectory planning techniques such as artificial potentials, potential fields, or graph-based methods to determine the best possible route, always considering the safety and efficiency of the robot's movement. This ensures that the robot can avoid obstacles effectively and autonomously and can adapt in real-time to changes in its environment to meet the navigation objectives proposed by the operator. In Figure 24, we see the result of the combination of the LIDAR and the RRT obstacle avoidance algorithm; this algorithm searches for a trajectory from a starting point to an established objective, avoiding obstacles in the environment defined by the LIDAR. The result of this can be seen in Figure 25, which is a visualization of how the robot interacts in a new environment; the algorithm expands the search tree, connects the nodes, and finally finds the optimal route to the objective. The simulation of the algorithm shows how the prototype moves between the points of the calculated trajectory.

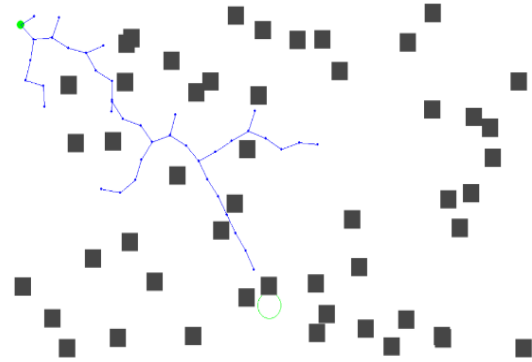


Fig. 24 RRT simulation

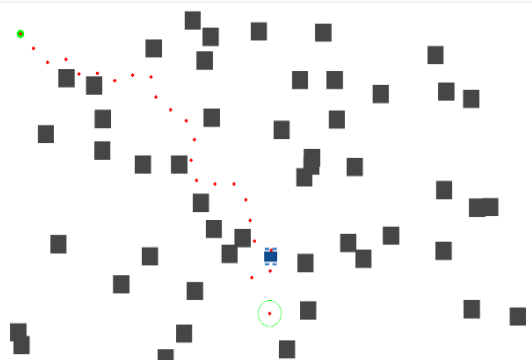


Fig. 25 RRT 2D environment simulation

This prototype also has a camera-operated manual driving system, which can be activated at any time from the control room (Figures 15 and 16), allowing operators to precisely and safely control the robot's operations in varied environments. The installed cameras provide a real-time view of the surrounding environment, allowing the operator to remotely monitor and guide the robot's actions. This capability is crucial for tasks requiring direct human intervention, such as delicate drill arm manipulation in sensitive areas or navigation through narrow or complex spaces. The transmission of high-resolution images and the possibility of using computer vision techniques allow the operator to perform precise and detailed actions, improving the safety and efficiency of operations (Figure 26).

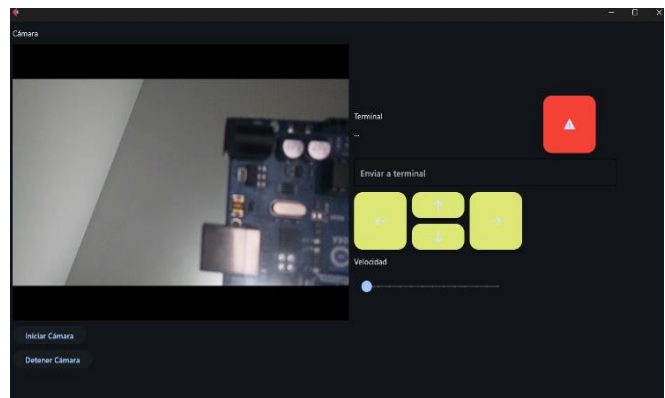


Fig. 26 Manual driving using the camera system

Once we finish with the sections of the mobile system, we proceed to the simulation of the drilling arm system. For this we will use Matlab and RoboDK. Figure 27 shows how the links work in 2D in the Matlab section. This was achieved by applying the equations of kinematics and dynamics and then using Simulink blocks to represent the joints and links of the robot. Subsequently, the desired trajectories for the end of the arm (end effector) were defined, and the control algorithms were implemented. In addition, Matlab offers us tools for 3D visualization of the movement of the robotic arm, which also allows us a detailed evaluation of its behavior and customization in different operating scenarios. To begin simulating in RoboDK, we must first be guided by the measurements between links obtained from the CAD software in Figure 28. A sketch was drawn above the model to obtain the required DH measurements requested by the RoboDK software to simulate. Figure 29 shows the CAD model in step format correctly loaded in the RoboDK simulator. The simulation in the RoboDK software allowed us to observe the robotic arm's behaviour in a virtual environment, allowing us to identify possible singularities and collisions of both the arm itself and its work area. Thanks to this tool, we were able to verify the movements' precision and thus adjust the optimization parameters that would ensure their performance in real situations.

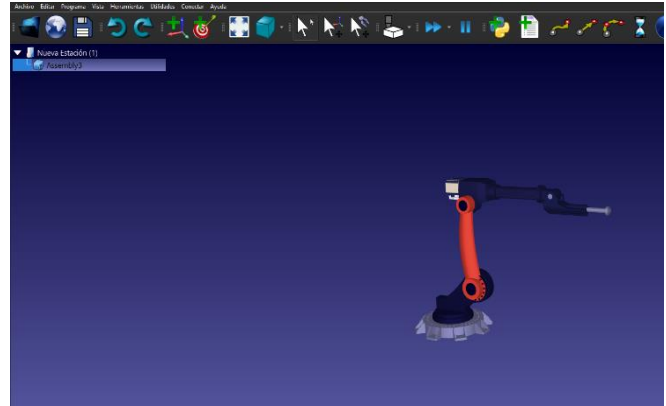


Fig. 29 Drilling arm in the RoboDK environment

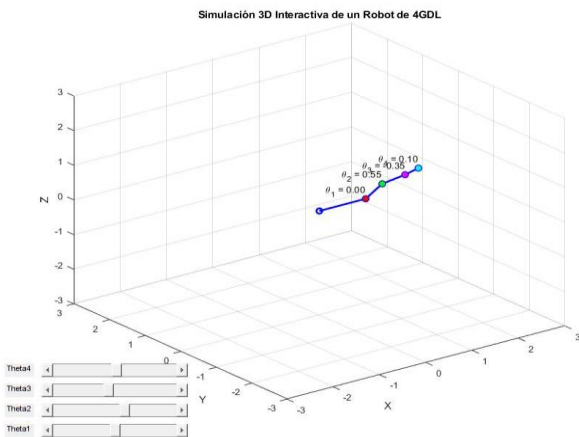


Fig. 27 2D simulation of the robot links

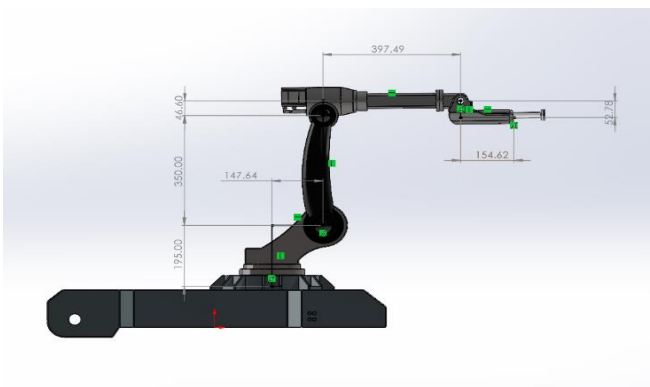


Fig. 28 DH arm measurements

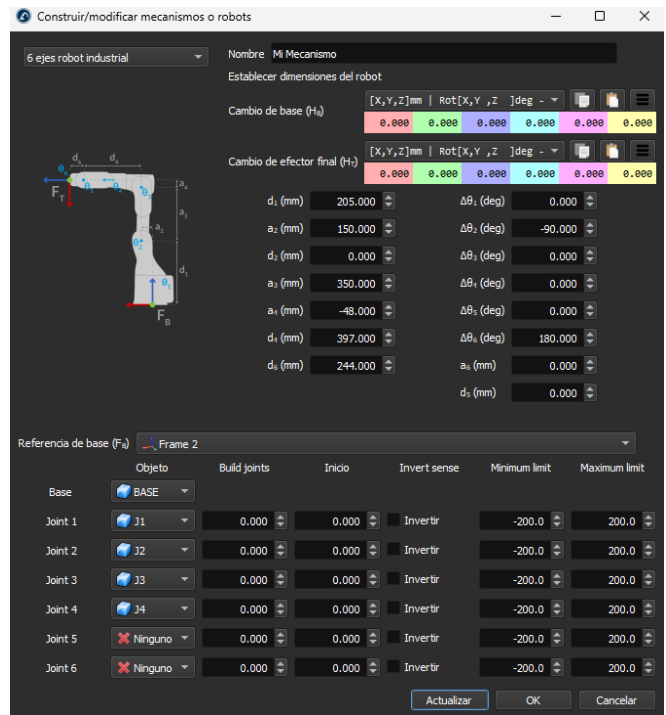


Fig. 30 Entering DH parameters to RoboDK.

In Figure 30, the data collected from Figure 28 correctly linked to their respective joints can be observed and thus be able to proceed with the control; the control interface can be seen in Figure 31. In the first part, we observe the robot's real-time position, and in the lower part, we simulate the desired movements. Figure 32 shows the final simulation of the robotic arm in RoboDK, where the configuration of its components' different positions and orientations can be seen. In the simulator interface, several options are presented to manipulate the robot, such as Cartesian and joint piloting, which allow the coordinates and angles of the arm joints to be adjusted to reach the desired positions as long as their limiting coordinates through mathematical models are known. In the simulation, due to the RoboDK license limitations, we were forced to use another similar 4GDL model from the RoboDK library, since the test license does not allow updating the base

axes of the joints, something vital for the simulation, which translates into the robot not moving as it should, in order to demonstrate the movement of the robot in a three-dimensional way we define 5 target points, P_START, P2, P1_DRILL, P2_DRILL, P3_DRILL, these points simulate the behavior of the robot when performing drilling a rock, taking advantage of these points as a basis, it was possible to determine the limitations and collisions with it and make the respective movement restrictions to offer better control.

3.2. Discussion

The results obtained in this study and prototype design are consistent with those obtained in previous works [3, 8, 10, 13, 15], where, through simulations, the desired responses were managed to be obtained. By applying the trajectory planning algorithms of [10, 13], the robot could go from point A to B autonomously. On the other hand, by applying the methodologies of [3, 8, 10], the robot could use the arm effectively in small spaces without generating collisions with it or with the environment.

The developed prototype of the mobile system with caterpillar traction, after being designed and simulated, obtained successful results in the control and design section that can be contrasted with the other studies [3, 22]; this means that the mathematical models and design proposed in this work were right ones. Trajectory planning and obstacle avoidance were critical components of the robot's success in confined environments. Using algorithms such as rapidly exploring random trees (RRT) allowed the robot to map its environment in real time and make autonomous decisions to avoid collisions. The results demonstrate that, as in [23, 24], the use of these algorithms favor the resolution of problems that may occur in established real-time environments.

4. Conclusion

In this work, a prototype of a manipulator mobile robot intended for drilling operations in underground mines has been developed and tested. The viability and efficiency of the system in controlled environments have been demonstrated through mathematical models and simulations. Integrating various sensors and control systems allows the robot to navigate autonomously and perform drilling tasks precisely, mitigating risks associated with human intervention in hostile environments. Simulation in RoboDK and practical implementation of the sensors have made it possible to identify and solve potential problems related to the singularity and collisions of the robotic arm. Additionally, the system's ability to operate in difficult underground conditions has been validated, showing robustness and adaptability suitable for mining applications.

Our results demonstrate that using robots in underground mining is possible and beneficial regarding safety and efficiency. Despite the limitations of budget, computing capacity, and sensors used, we believe that the lessons learned and improvements made during the development of this prototype provide a solid foundation for future work and applications. Furthermore, it is noted that integrating advanced technologies such as artificial intelligence and machine learning could further optimize the robot's capabilities. Implementing mobile manipulator robots can revolutionize the Peruvian mining industry and significantly improve working conditions and productivity. This could not only reduce risk to human workers but also increase precision and efficiency in mining operations.

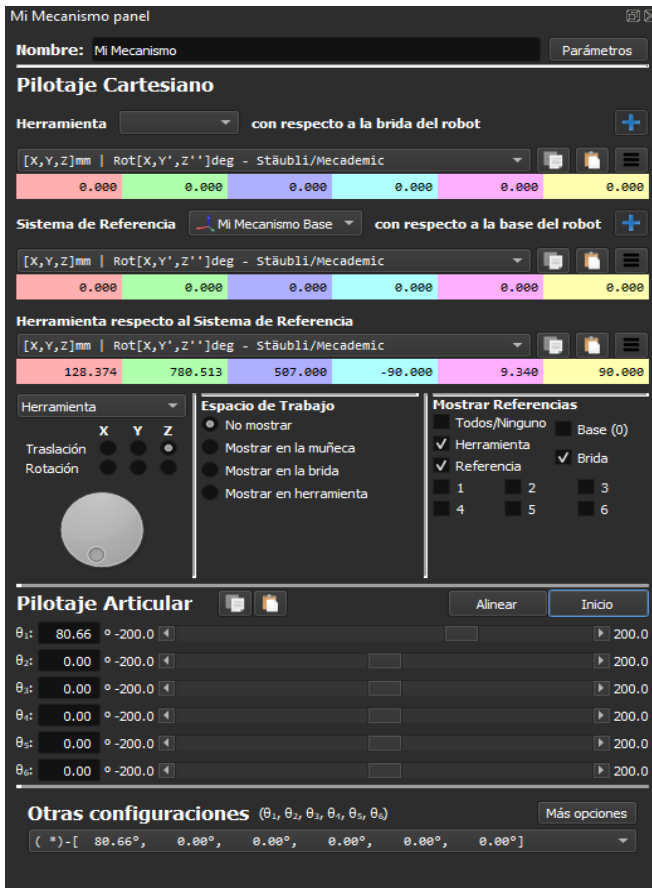


Fig. 31 Simulation section in RoboDK

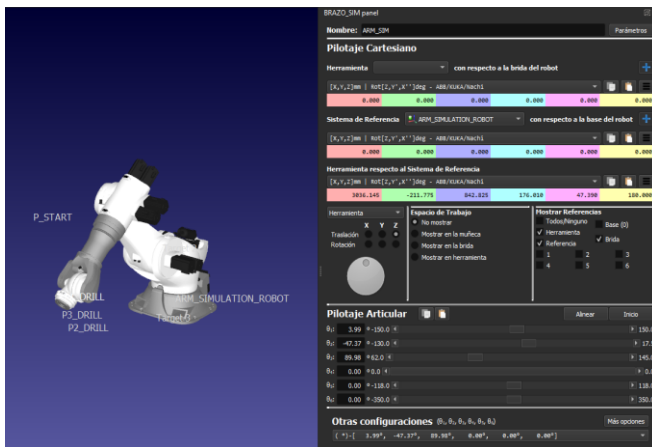


Fig. 32 Final simulation of the drilling arm

References

- [1] Mining Represents Almost he 15% of the GDP National by Activity Same and Impact in Others Sectors, Stated MINEM, Iimp, 2022. [Online]. Available: <https://iimp.org.pe/raiz/mineria-representa-casi-el-15-del-pbi-nacional-por-actividad-misma-e-impacto-en-otros-sectores-afirmo-minem>
- [2] Ministry of Energy and Mines, Minem, 2022. [Online]. Available: <https://www.gob.pe/minem>
- [3] Joseph Nsasi Bakambu, and Vladimir Polotski, “Autonomous System for Navigation and Surveying in Underground Mines,” *Journal of Field Robotics*, vol. 24, no. 10, pp. 829-847, 2007. [[CrossRef](#)] [[Google Scholar](#)] [[Publisher Link](#)]
- [4] W. Pratt Rogers et al., “Automation in the Mining Industry: Review of Technology, Systems, Human Factors, and Political Risk,” *Mining, Metallurgy & Exploration*, vol. 36, pp. 607-631, 2019. [[CrossRef](#)] [[Google Scholar](#)] [[Publisher Link](#)]
- [5] Ashutosh Kumar Singh, and Shahzad Ali, “A Research on Use of Robotics in Mining Industry,” *International Journal of Recent Technology and Engineering*, vol. 8, no. 2S11, pp. 2091-2093, 2019. [[CrossRef](#)] [[Publisher Link](#)]
- [6] Ministry of Energy and Mines, *Occupational Health and Safety Regulations in Mining*, 2020. [[Google Scholar](#)] [[Publisher Link](#)]
- [7] Zhang Jun et al., “Design and Workspace Analysis of Drilling Arm of Mining Anchor Drilling Robot,” *Journal of Physics: Conference Series, The 2022 International Conference on Applied Mathematics and Computational Mechanics*, Virtual, China, vol. 2202, no. 1, pp. 1-10, 2022. [[CrossRef](#)] [[Google Scholar](#)] [[Publisher Link](#)]
- [8] Gonzalo J. Paz-Delgado et al., “Combined Path and Motion Planning for Workspace Restricted Mobile Manipulators in Planetary Exploration,” *IEEE Access*, vol. 11, pp. 78152-78169, 2023. [[CrossRef](#)] [[Google Scholar](#)] [[Publisher Link](#)]
- [9] Renato Vidoni et al., “Evaluation and Stability Comparison of Different Vehicle Configurations for Robotic Agricultural Operations on Side-Slopes,” *Biosystems Engineering*, vol. 129, pp. 197-211, 2015. [[CrossRef](#)] [[Google Scholar](#)] [[Publisher Link](#)]
- [10] Tran Thanh Tung et al., “Development of a Prototype 6 Degree of Freedom Robot Arm,” *Results in Engineering*, vol. 18, 2023. [[CrossRef](#)] [[Google Scholar](#)] [[Publisher Link](#)]
- [11] Umberto Montanaro et al., “Multi-Input Enhanced Model Reference Adaptive Control Strategies and their Application to Space Robotic Manipulators,” *International Journal of Robust and Nonlinear Control*, vol. 33, no. 10, pp. 5246-5272, 2023. [[CrossRef](#)] [[Google Scholar](#)] [[Publisher Link](#)]
- [12] Shipeng Wang et al., “Optical-Nanofiber-Enabled Gesture-Recognition Wristband for Human-Machine Interaction with the Assistance of Machine Learning,” *Advanced Intelligent Systems*, vol. 5, no. 7, 2023. [[CrossRef](#)] [[Google Scholar](#)] [[Publisher Link](#)]
- [13] Shaobo Zhang et al., “Multi-Objective Optimal Trajectory Planning for Robotic Arms Using Deep Reinforcement Learning,” *Sensors*, vol. 23, no. 13, pp. 1-15, 2023. [[CrossRef](#)] [[Google Scholar](#)] [[Publisher Link](#)]
- [14] Min Zhang et al., “Modification Technique for a Space Manipulator Joint’s Thermal Model Parameter,” *Case Studies in Thermal Engineering*, vol. 49, 2023. [[CrossRef](#)] [[Google Scholar](#)] [[Publisher Link](#)]
- [15] Wang Minchuan, “Self-Compensation Method for Error of Positioning Accuracy of Intelligent Synchronous Manipulator,” *Thermal Science*, vol. 24, no. 3, pp. 1569-1576, 2020. [[CrossRef](#)] [[Google Scholar](#)] [[Publisher Link](#)]
- [16] Mark W. Spong, Seth Hutchinson, and M. Vidyasagar, *Robot Modeling and Control*, 2nd ed., Jhon Wiley & Sons, pp. 1-608, 2020. [[Google Scholar](#)] [[Publisher Link](#)]
- [17] Hong-Xing Wei et al., “Inverse Dynamic Modeling and Analysis of a New Caterpillar Robotic Mechanism by Kane’s Method,” *Robotica*, vol. 31, no. 3, pp. 493-501, 2013. [[CrossRef](#)] [[Google Scholar](#)] [[Publisher Link](#)]
- [18] Nelson Arzola, and Gonzalo Rojas, “Analysis of the Dynamic Behavior of a Vehicle with Independent Deformable Parallelogram Suspension and Transverse Stability Bars,” *Journal of the Faculty of Engineering, University of Antioquia*, no. 67, pp. 112-125, 2013. [[CrossRef](#)] [[Google Scholar](#)] [[Publisher Link](#)]
- [19] Bhag S. Guru, and Huseyin R. Hiziroglu, *Electric Machinery and Transformer*, Oxford University Press, pp. 1-700, 2007. [[Google Scholar](#)] [[Publisher Link](#)]
- [20] Richard Gordon Budynas, and J. Keith Nisbett, *Shigley’s Mechanical Engineering Design*, McGraw-Hill Education, pp. 1-1082, 2016. [[Google Scholar](#)] [[Publisher Link](#)]
- [21] Vito Antonio Nardi, Alessia Ferraro, and Valerio Scordamaglia, “Feasible Trajectory Planning Algorithm for a Skid-Steered Tracked Mobile Robot Subject to Skid and Slip Phenomena,” *2018 23rd International Conference on Methods & Models in Automation & Robotics, Miedzyzdroje, Poland*, pp. 120-125, 2018. [[CrossRef](#)] [[Google Scholar](#)] [[Publisher Link](#)]
- [22] W. Pratt Rogers et al., “Automation in the Mining Industry: Review of Technology, Systems, Human Factors, and Political Risk,” *Mining, Metallurgy & Exploration*, vol. 36, pp. 607-631, 2019. [[CrossRef](#)] [[Google Scholar](#)] [[Publisher Link](#)]
- [23] Valerio Scordamaglia, and Vito Antonio Nardi, “A Set-Based Trajectory Planning Algorithm for a Network Controlled Skid-Steered Tracked Mobile Robot Subject to Skid and Slip Phenomena,” *Journal of Intelligent & Robotic Systems*, vol. 101, 2021. [[CrossRef](#)] [[Google Scholar](#)] [[Publisher Link](#)]
- [24] Jeremy Green, “Underground Mining Robot: A CSIR Project,” *2012 IEEE International Symposium on Safety, Security, and Rescue Robotics*, College Station, TX, USA, pp. 1-6, 2012. [[CrossRef](#)] [[Google Scholar](#)] [[Publisher Link](#)]